研究成果の刊行に関する一覧表

	発表者氏名	論文タイトル	発表誌名	巻号	ページ	出版年
1	Lee HS,Homma A, Tatsumi E, Taenaka Y	Observation of cavitation pits on mechanical heart valve surfaces in an artificial heart used in in vitro testing	J Artificial Organs	13	17-23	2010
2	Lee HS,Tatsumi E, Taenaka Y	Flow Visualization of a monoleaflet and bileaflet mechanical heart valve in a pneumatic ventricular assist device using a PIV system	ASAIO Journal	56(3)	186-193	2010
3	金城利晴、李 桓成、巽 英介、妙中義之、上村匡敬	二葉式機械弁を用いた空気駆動式補助人工心臓内部における流れの可視化	日本機械学会講演論文集	104(1)	18-9	2010
4	築谷朋典、巽 英介、妙中義之、大久保 剛、長田俊幸、山根隆志	体内埋め込み型補助人工心臓用軸流ポンプの生体適合性評価	第22回バイオエンジニアリング講演会講演論文集		55	2010
5	妙中義之	医療機器の研究開発の促進への取り組み -先端医療開発特区（スーパー特区）の構築-	医薬品医療機器レギュラトリーサイエンス	41(8)	611-617	2010
6	築谷朋典、水野敏秀、巽 英介、妙中義之、西中知博、山嵜健二	左室心尖部より挿入される補助人工心臓脱血管の形状に関する流体工学的検討	日本機械学会2010年度年次大会講演論文集（講演論文集Vol. 6）		157-158	2010
7	大沼健太郎、本間章彦、住倉博仁、妙中義之、巽 英介、赤川英毅、武輪能明、水野敏秀、築谷朋典、片桐伸将、角田幸秀、下崎 勇生、向林 宏、片野一夫	空気駆動式人工心臓の流量推定に関する検討	電気学会研究会資料	LD-10	51-55	2010
8	本間章彦、住倉博仁、大沼健太郎、妙中義之、巽 英介、武輪能明、赤川英毅、水野敏秀、築谷朋典、片桐伸将、角田幸秀、福井康裕、下崎勇生、向林 宏、片野一夫	空気駆動式ウェアラブル全人工心臓システムの開発	電気学会研究会資料	LD-10	57-61	2010
9	Yamane T,Kyo S, Matsuda H, Abe Y, Imachi K, Masuzawa T, Nakatani T, Sase K, Tabayashi K, Takatani S, Tatsumi E, Umezu M, Tsuchiya T	Japanese guidance for ventricular assist devices/Total artificial hearts	Artificial Organs	34(9)	699-702	2010

10	Sawa Y,Tatsumi E, Funakubo A, Horiuchi T, Iwasaki K, Kishida A, Masuzawa T, Matsuda K, Myoui A, Nishimura M, Nishimura T, Tomizawa Y, Tomo T, Yamaoka T, Watanabe H	Journal of Artificial Organs 2009: the year in review	J Artif Organs	13(1)	1-9	2010
11	巽 英介	人工肺の研究開発・臨床応用	人工臓器2010 第26回日本人工臓器学会教育セミナー			2010
12	巽 英介	次世代型人工心臓の開発と臨床応用	応用物理	80(2)	110-115	2011
13	武輪能明	心室内形状を考慮した、心拍動下に装着可能な低侵襲性かつ抗血栓性補助循環脱血カニューラの開発	人工臓器	39(1)	38-39	2010
14	Kawada T, Shimizu S, Kamiya A, Sata Y, Uemura K, Sugimachi M.	Dynamic characteristics of baroreflex neural and peripheral arcs are preserved in spontaneously hypertensive rats.	Am J Physiol Regul Integr Comp Physiol.	300(1)	R155-R165	2011
15	Yamamoto H, Kawada T, Kamiya A, Miyazaki S, Sugimachi M. Auton Neurosci.	Involvement of the mechanoreceptors in the sensory mechanisms of manual and electrical acupuncture.	Auton Neurosci.	160(1-2)	27-31	2011
16	Kamiya A, Kawada T, Mizuno M, Shimizu S, Sugimachi M.	Parallel resetting of arterial baroreflex control of renal and cardiac sympathetic nerve activities during upright tilt in rabbits.	Am J Physiol Heart Circ Physiol.	298(6)	H1966-H1975	2010
17	Kawada T, Li M, Kamiya A, Shimizu S, Uemura K, Yamamoto H, Sugimachi M.	Open-loop dynamic and static characteristics of the carotid sinus baroreflex in rats with chronic heart failure after myocardial infarction.	J Physiol Sci.	60(4)	283-298	2010
18	Mizuno M, Kawada T, Kamiya A, Miyamoto T, Shimizu S, Shishido T, Smith SA, Sugimachi M.	Dynamic characteristics of heart rate control by the autonomic nervous system in rats.	Exp Physiol.	95(9)	919-925	2010
19	Sugimachi M, Sunagawa K, Uemura K, Shishido T.	Physiological significance of pressure-volume relationship: A load-independent index and a determinant of pump function.	Conf Proc IEEE Eng Med Biol Soc.	1	3553.	2010

20	Sugimachi M, Sunagawa K, Uemura K, Kamiya A, Shimizu S, Inagaki M, Shishido T.	Estimated venous return surface and cardiac output curve precisely predicts new hemodynamics after volume change.	Conf Proc IEEE Eng Med Biol Soc.	1	5205-5208	2010
21	unagawa K, Sugimachi M.	Development of artificial bionic baroreflex system.	Conf Proc IEEE Eng Med Biol Soc.	1	3446-3448	2010
22	Uemura K, Sugimachi M, Kawada T, Sunagawa K.	Automated drug delivery system for the management of hemodynamics and cardiac energetic in acute heart failure.	Conf Proc IEEE Eng Med Biol Soc.	1	5222-5225.	2010
23	Uemura K, Zheng C, Li M, Kawada T, Sugimachi M.	Early short-term vagal nerve stimulation attenuates cardiac remodeling after reperfused myocardial infarction.	J Card Fail.	16(8)	689-699	2010
24	S. Kakinoki and T. Yamaoka,	Stable modification of poly(lactic acid) surface with neurite outgrowth-promoting peptides via hydrophobic collagen-like sequence,	Acta Biomaterialia,	6	1925-1930	2010
25	A. Mahara and T. Yamaoka,	Antibody-immobilized column for quick cell separation based on cell rolling,	Biotecnology Progress	26(2)	441-447	2010
26	A. Miskon, A. Mahara, H. Uyama, and T. Yamaoka,	A suspension induction for myocardial differentiation of rat mesenchymal stem cells on various ECM proteins,	Tissue Engineering Part C,	doi:10.1089/ten.tec.2009	218	2010
27	A. Mahara and T. Yamaoka,	Continuous separation of cells of high osteoblastic differentiation potential from mesenchymal stem cells on an antibody-immobilized column,	Biomaterials,	31	4231-4237	2010
28	T. Ehashi, A. Nishigaito, T. Fujisato, Y. Moritan, and T. Yamaoka,	Periferal nerve regeneration and electrophysiological recovery with CIP-treated allogeneic acellular nerve	J. Biomat. Sci.	22	627-640	2011
29	Y. Tachibana, J. Enmi, A.Mahara, H. Iida, and T. Yamaoka,	Design and characterization of a polymeric MRI contrast agent based on PVA for in vivo living-cell tracking	Contrast Media and Molecular Imaging,	5	309-317	2010

30	S. Kakinoki, S. Uchida, T. Ehashi, A. Murakami, and T. Yamaoka,	Preipheral nerve regeneration using PLA nanofiber conduit modified with neurite outgrowth promoting peptide-oligo(lactic acid)conjugates in the rat,	Peptide Science	2009	409-410	2010
31	Y. Tachibana, T. Hashimoto, H. Nozaki, A. Murakami, T. Yamaoka	Timing-controlled Decompaction of Polyplexes In Vivo Greatly Enhances Transgene Expression,	Chem. Lett.,	39	1238-1239	2010
32	Agudelo CA, Tachibana Y, Noboru T, Iida H, Yamaoka T.	Long term in vivo MRI tracking of endothelial progenitor cells transplanted in rat ischemic limbs and their angiogenic potential.	Tissue Eng Part A.	2011 Apr 6		2011
33	S. Kakinoki, S. Uchida, T. Ehashi, A. Murakami, T. Yamaoka,	Surface modification of poly(L-lactic acid) nanofiber with oligo(D-lactic acid)–bioactive-peptide conjugates for peripheral nerve regeneration,	Polymers	3(2)	820-832	2011

J Artif Organs (2010) 13:17–23
DOI 10.1007/s10047-010-0490-3

ORIGINAL ARTICLE

Observation of cavitation pits on mechanical heart valve surfaces in an artificial heart used in in vitro testing

Hwansung Lee · Akihiko Homma · Eisuke Tatsumi · Yoshiyuki Taenaka

Received: 11 May 2009 / Accepted: 5 January 2010 / Published online: 13 February 2010

Abstract Our group has developed an electrohydraulic total artificial heart (EHTAH) with two diaphragm-type blood pumps. Cavitation in a mechanical heart valve (MHV) causes valve surface damage. The objective of this study was to investigate the possibility of estimating the MHV cavitation intensity using the slope of the driving pressure just before valve closure in this artificial heart. Twenty-five and twenty-three-millimeter Medtronic Hall valves were mounted at the inlet and outlet ports, respectively, of both pumps. The EHTAH was connected to the experimental endurance tester developed by our group, and tested under physiological pressure conditions. Cavitation pits could be seen on the inlet valve surface and on the outlet valve surface of the right and left blood pumps. The pits on the inlet valves were more severe than those on the outlet valves in both blood pumps, and the cavitation pits on the inlet valve of the left blood pump were more severe than those on the inlet valve of the right blood pump. The longer the pump running time, the more severe the cavitation pits on the valve surfaces. Cavitation pits were concentrated near the contact area with the valve stop. The major cause of these pits was the squeeze flow between the leaflet and valve stop.

H. Lee (✉) · A. Homma · E. Tatsumi · Y. Taenaka
Department of Artificial Organs, Research Institute, National Cardiovascular Center, 5-7-1 Fujishiro-dai, Suita, Osaka 565-8565, Japan
e-mail: hslee@ri.ncvc.go.jp

Keywords Electrohydraulic total artificial heart · Endurance testing · Mechanical heart valve · Cavitation pits

Introduction

In previous studies we investigated mechanical heart valve (MHV) cavitation in an electrohydraulic total artificial heart (EHTAH) [1], and we reported the mechanism for MHV cavitation and the cavitation intensity. We also observed the generation, growth and collapse of cavitation bubbles near one of the heart's valve stops after valve closure. When cavitation occurs near the material surface of a MHV, this rapid collapse may cause a high-speed micro-jet and shock waves, which cause cavitation on the valve surface [2, 3]. Microscopic pitting was observed on the leaflet surface and hinge of a MHV after implantation, and this pitting might be causing the cavitation phenomenon [4–6]. Dexter et al. [7] reported negative pressure below the vapor pressure near the leaflet in an animal experiment.

The flow through the major orifice of the tilting disc valve acts on the diaphragm-housing junction of the blood pump [8], and this creates a washout effect inside the blood pump that helps to prevent thrombosis. For this reason we selected the Medtronic Hall valve for use in our EHTAH. In this study, we investigated the possibility of cavitation of the Medtronic Hall valve during in-vivo testing using our EHTAH. In an earlier study, even if there was no significant hemolysis, cavitation pits could be found on the valve surface near the valve stop [9]. In addition to this result, the cavitation pits can more severe with long-term use.

In this study, we investigated cavitation pits of the MHV surface using a durability test in a long-term experiment to investigate the durability of the MHV in our EHTAH.

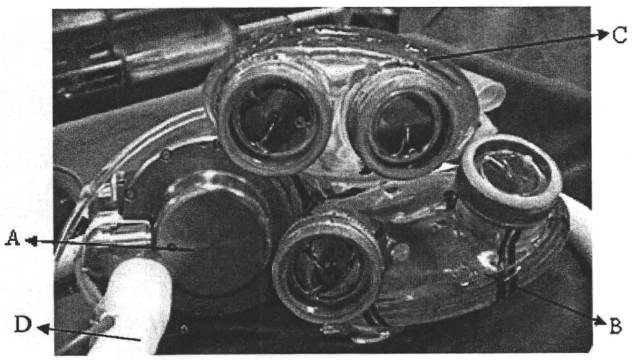

Fig. 1 The electrohydraulic total artificial heart. **a** actuator, **b** right blood pump, **c** left blood pump, **d** control cable

Materials and methods

The EHTAH we developed consists of two diaphragm-type blood pumps [9], an actuator and a controller (Fig. 1). The actuator is connected to both blood pumps, which are filled with silicon oil. The silicon oil drives the blood pump by the forward and/or reverse rotation of the impeller inside the actuator. The revolutionary speed of the impeller and the systolic ratio are controlled by the controller. The total volume of the left and right blood pumps was 390 mL, and the pumps have a stroke volume of 75 mL. Twenty-five and twenty-three-millimeter Medtronic Hall valves (Medtronic, Minneapolis, MN, USA) were mounted at the inlet and outlet ports, respectively, of both blood pumps (Fig. 1).

The EHTAH was connected to the endurance experiment tester under physiological pressure conditions developed by our group (Fig. 2). It was placed in physiological saline at 36°C. The EHTAH consists of four chambers, a right atrium chamber, a pulmonary chamber, an arterial chamber, and a left atrium chamber. In the case of the right blood pump, fluid flows from the right atrium chamber (RA) into the right blood pump and is then pumped into the pulmonary arterial chamber (PA). In the case of the left blood pump, fluid flows from the left atrium chamber (LA) into the aortic chamber (Ao) (Fig. 2). The pump rate was fixed at 80 and 120 bpm, and the left systolic ratio was fixed at 50%. The motor revolution speed was 1,100 rpm for the left systole and 900 rpm for the right systole (Table 1). Cavitation pits on the valve surface were compared for three different sets of running conditions—valve-closure cycles of 40.78, 89.16, and 134.26 $\times$ 10^6 cycles (Table 1).

As working fluid, tap water at 36°C was used. A pressure transducer (PA-500; Copal Electronics, Tokyo, Japan) was used to measure the driving pressure of the right and left blood pumps.

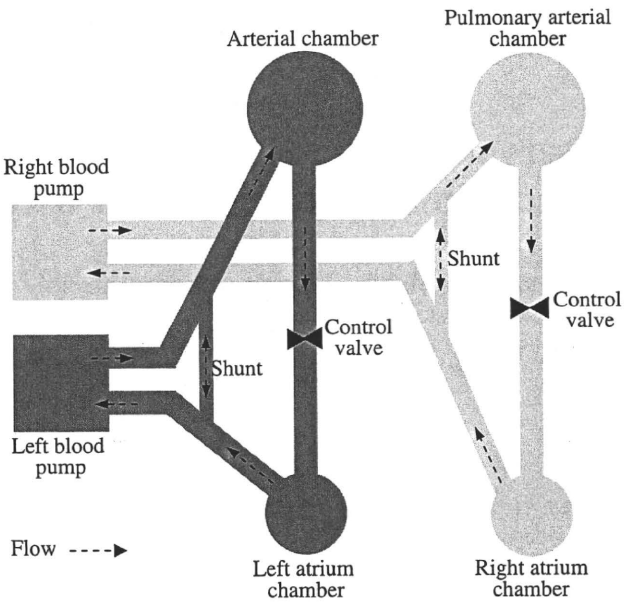

Fig. 2 Mechanism for endurance testing of the electrohydraulic total artificial heart

Results

Three endurance tests were stopped by the seal failure of the pump. When this happened the valve-closure cycle ranged from 40.78 to 134.26 $\times$ 10^6 cycles (equal to 354–1,165 days for normal conditions of 80 bpm). Throughout the testing, the mean left atrium and mean aortic pressures were maintained at 10 and 110 mmHg, respectively, and the mean right atrium and mean pulmonary artery pressures were maintained at 10 and 30 mmHg, respectively (Fig. 3).

The maximum left driving pressure (LDP) and right driving pressure (RDP) reached 320 and 100 mmHg, respectively (Fig. 4), and the minimum LDP and RDP reached −80 and −100 mmHg, respectively. The EHTAH was run by an actuator, which drives the blood pump by using silicone oil to conduct movement via forward and/or reverse rotation of the impeller. The left and right blood pumps were alternately filled and emptied by the actuator causing displacement of the diaphragms. In the case of full-filling and full-emptying conditions for the left blood pump, the diaphragm was pulled and pushed by the silicon oil force, and hence the negative (points "A" and "D" of Fig. 4) and positive (points "B" and "E" of Fig. 4) peak pulse pressure was generated. During the LDP and RDP waves, the slope of the pressure increased suddenly during the systolic phase (points "C" and "F" of Fig. 4). In a previous study, we estimated that this point might be the valve-closure point [1]. Even with the blood pump operating under stable conditions, the LDP slope 5 ms before valve closure was irregular (points "C" and "F" of Fig. 4), ranging from 7,000 to 13,000 mmHg/s. On the other hand,

Table 1 EHTAH running conditions for pump endurance testing

Case no.	Running time (days)	Heart rate (beats/min)	Motor revolution speed for the left systole (rpm)	Motor revolution speed for the right systole (rpm)	Left systolic duration (%)	Number of the valve closure cycle ($\times 10^6$)	Event
1	354	80	1,100	900	50	40.78	Seal failure
2	774	80	1,100	900	50	89.16	Seal failure
3	777	120	1,100	900	50	134.26	Seal failure

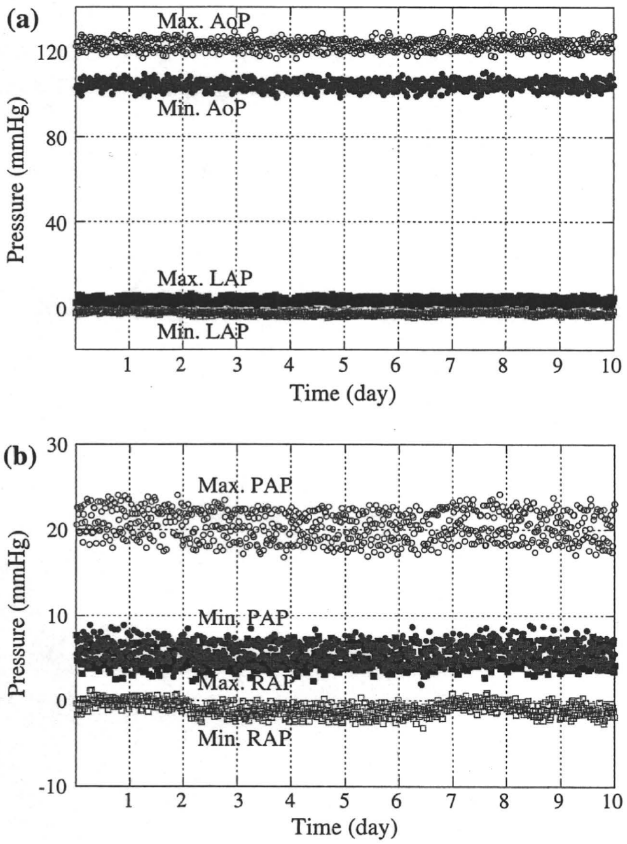

Fig. 3 Pressure waves at a heart rate of 80 bpm. **a** Aortic pressure and left atrial pressure, **b** pulmonary artery pressure and right atrial pressure. *Max. AoP* maximum aortic pressure, *Min. AoP* minimum aortic pressure, *Max. LAP* maximum left atrial pressure, *Min. LAP* minimum left atrial pressure, *Max. PAP* maximum pulmonary artery pressure, *Min. PAP* minimum pulmonary artery pressure, *Max. RAP* maximum right atrial pressure, *Min. RAP* minimum right atrial pressure

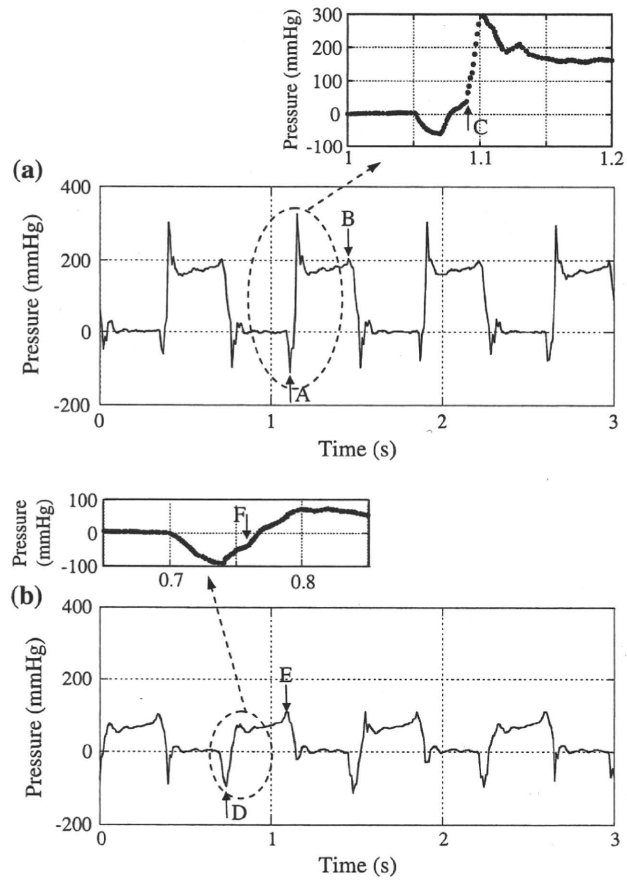

Fig. 4 The left driving pressure (LDP) and right driving pressure (RDP) waves at a heart rate of 80 bpm

the RDP slope 5 ms before valve closure pressure change ranged from only 5,200 to 8,500 mmHg/s.

A photograph of the valve surface after endurance testing is shown in Fig. 5. This valve was run at a heart rate of 80 bpm for 354 days of running time. Cavitation pit marks were found to be concentrated on the area in contact with the valve stop (Fig. 5). Enlarged photographs of the cavitation pits appear in Figs. 6, 7, 8. The cavitation pits could be seen on the inlet valve surface and the outlet valve surface of the right and left blood pumps, and the pits of the inlet valves were more severe than those of the outlet valves in both blood pumps (Figs. 6, 7, 8). The cavitation pits of the inlet valve of the left blood pump were more severe than those of the inlet valve of the right blood pump (Figs. 6, 7, 8). The intensity of the cavitation pits increased with increasing number of valve-closure cycles. The large cavitation pits were over 3 μm in diameter (Figs. 6, 7, 8).

Discussion

In general, the causes of cavitation in MHVs include the Venturi effect caused by flow after valve closure in the

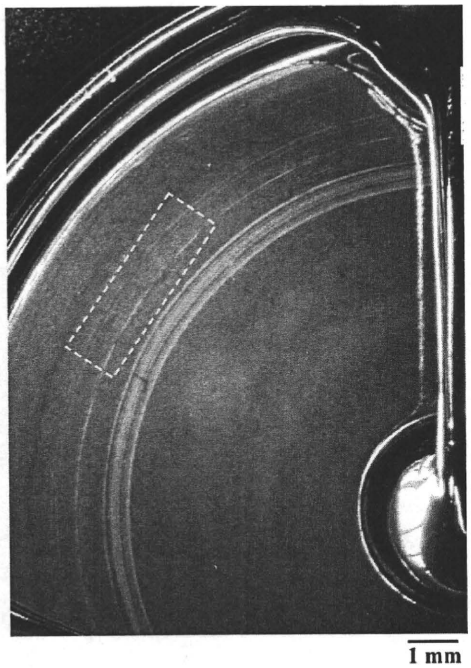

Fig. 5 Photograph of the valve surface after endurance testing. This valve was run at a heart rate of 80 bpm for 354 days of running time

narrow gap between the leaflet and valve housing, the water hammer effect caused by the sudden stop of the valve, and the squeeze flow that can occur in the narrow gap between the leaflet and valve stop during the final period of valve closure [10–14]. In a previous study, we observed cavitation pits on the valve surface where it contacted the valve stop in in-vivo testing [9]. In our latest study we conducted endurance testing for over 1 year, and most of the cavitation pits were observed near the area in contact with the valve stop (Figs. 6, 7, 8). This means that the major cause of MHV cavitation is the squeeze flow. The squeeze flow velocity is proportional to the valve-closure velocity and the area of the valve stop [14]. In theory, when the squeeze flow velocity is faster than 14 m/s ($u = (2p/\rho)^{1/2} = 14$ m/s), the pressure falls below the vapor pressure of the working fluid, and then cavitation bubbles are generated [14]. When cavitation occurs near the material surface of an MHV, this rapid collapse may cause a high-speed micro-jet and shock waves, which cause cavitation pits on the valve surface. The larger the cavitation pits observed near the valve stop, the longer the valve-closure cycle (Fig. 8). This suggests overlapping multiple sessions of cavitation pitting, which raises the possibility that wider cavitation pits form with long-term exposure to cavitation.

As in the previous study [9], both the LDP slope and RDP slope at 5 ms before valve closure exceeded the cavitation threshold (Fig. 4) in our latest study. The LDP slope was larger than that of the RDP, which means that the inlet valve-closing velocity of the left blood pump was higher than that of the right blood pump. This was the major reason why stronger and larger cavitation pits were generated in the inlet of the left blood pump than in the inlet of the right blood pump (Figs. 6, 7, 8). This means that the high slope of the driving pressure led to an increase in not only the number of cavitation pits but also the area in which the cavitation pits occurred. In a previous study, we confirmed the possibility of cavitation at the outlet valve of an artificial heart [15]. Even if the RMS pressure caused by cavitation of the outlet valve was less than that of the inlet valve, there is a possibility of cavitation at the outlet valve [15]. Moreover, the valve was closed by the pressure difference between the after-load and the ventricular pressure, and its pressure difference correlated with the cavitation intensity [15]. As shown in Fig. 3, the after-load of the outlet valve of the right blood pump was less than that of the left blood pump, which might have reduced the cavitation pits near the outlet valve of the right blood pump.

In order to estimate the endurance for not only the MHV but also the EHTAH, the EHTAH was placed in physiological saline at 36°C. Moreover, because of the difficulty of maintaining fluid viscosity, caused by the vaporization of the water, in this study we used tap water as the working fluid. It differs from blood at body temperature in viscosity and vapor pressure. Graf et al. [16] reported that cavitation thresholds obtained in the pulsatile mock loop with tap water were lower than those in whole blood. Therefore, when an artificial heart is implanted in a human, more severe cavitation pits than those generated in this study may occur. To try to prevent this problem, we experimented with a variety of working fluids [1]. The probability of occurrence of cavitation was higher for tap water than for glycerine solution, which has the same viscosity and vapor pressure as blood. This means that tap water contains particles that cause an increase in the probability of occurrence of cavitation. Accordingly, we believe that blood, which contains a variety of particles, for example red cells, lymphocytes, and monocytes, can play a crucial role in the induction and course of cavitation.

In general, the concentration of the P_{CO_2} is important for the rate of growth of gas bubbles [17]. In a previous study the EHTAH was connected to the Donovan mock loop tester with a rigid tube, and the relationship between cavitation intensity and the P_{CO_2} was investigated using glycerine solution as the working fluid [18]. We found no significant difference between the P_{CO_2} and the cavitation intensity in an EHTAH [18]. Because the MHVs mounted in the EHTAH close much faster than in ordinary use, a more rapid squeeze flow occurred surrounding the valve stop. In this study, the EHTAH was connected to the

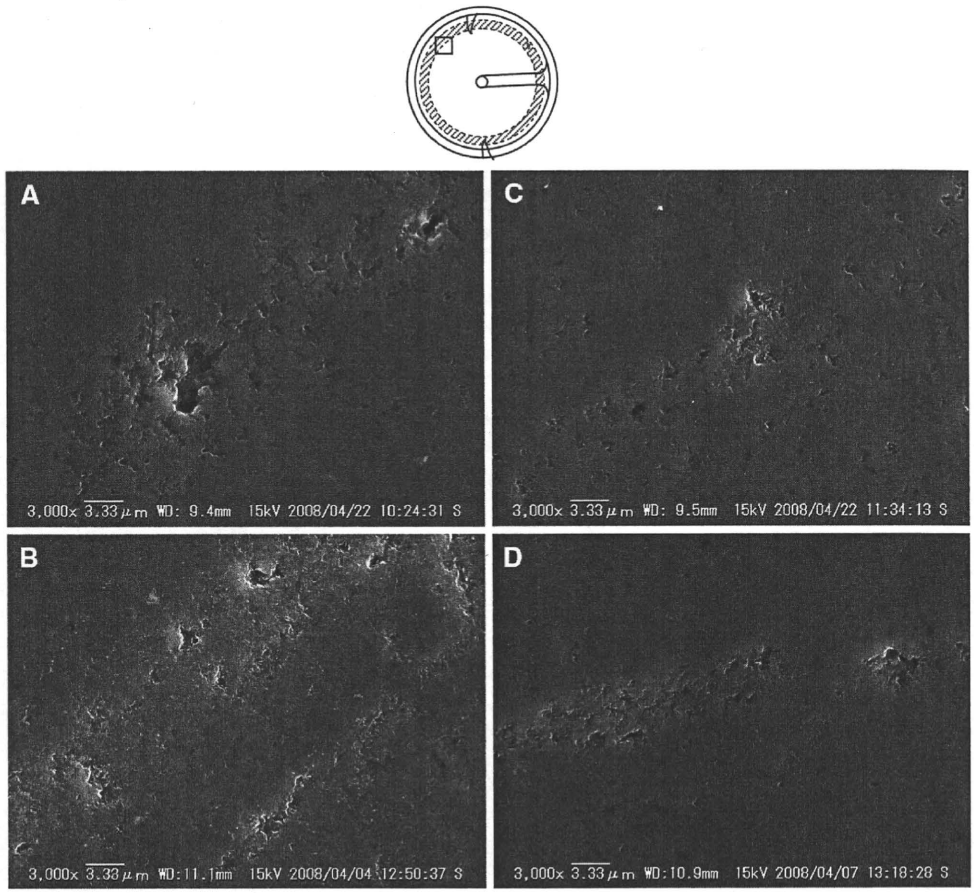

Fig. 6 Scanning electron micrograph of the valve surface run at a heart rate of 80 bpm for 354 days of running time. **a** Inlet valve surface of the left blood pump, **b** outlet valve surface of the left blood pump, **c** inlet valve surface of the right blood pump, **d** outlet valve surface of the right blood pump

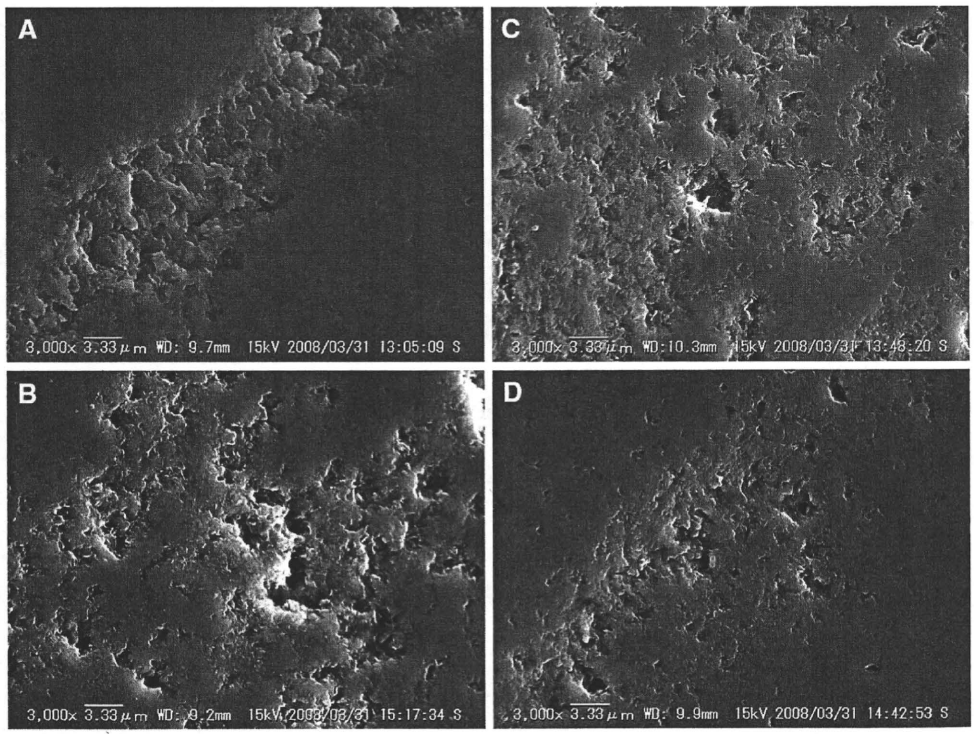

Fig. 7 Scanning electron micrograph of the valve surface run at a heart rate of 80 bpm for 774 days of running time. **a** Inlet valve surface of the left blood pump, **b** outlet valve surface of the left blood pump, **c** inlet valve surface of the right blood pump, **d** outlet valve surface of the right blood pump

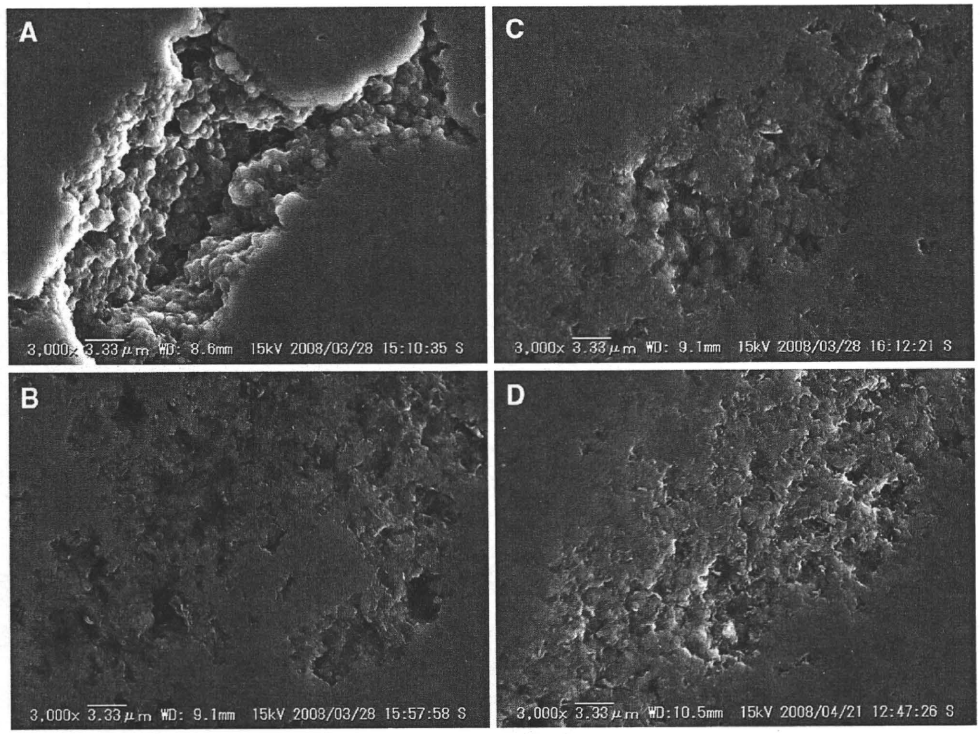

Fig. 8 Scanning electron micrograph of the valve surface run at a heart rate of 120 bpm for 777 days of running time. **a** Inlet valve surface of the left blood pump, **b** outlet valve surface of the left blood pump, **c** inlet valve surface of the right blood pump, **d** outlet valve surface of the right blood pump

experimental endurance tester, and thus it did not have as much compliance as the blood vessels. From this fact, the effect of the gas concentration on cavitation pits might be ignored when using the experimental endurance tester.

Conclusions

In this study we investigated cavitation pits on the MHV surface using endurance testing in a long-term experiment. Cavitation pits appeared on the inlet valve surface and on the outlet valve surface of the right and left blood pumps, concentrated near the area in contact with the valve stop. The major cause of these pits is the squeeze flow between the leaflet and valve stop. The LDP slope was larger than that of the RDP, and there was a tendency for the cavitation pits on the inlet valve of the left blood pump to be more severe than those of the right blood pump. The longer the pump running time, the more severe the cavitation pits observed in both valve surfaces.

References

1. Lee HS, Taenaka Y, Kitamura S. Mechanism for cavitation in the mechanical heart valve with an artificial heart: nuclei and viscosity dependence. Artif Organs. 2005;29:41–6.
2. Knapp RT, Daily JW, Hammitt FG. Cavitation. Iowa City: Institute of Hydraulic Research, University of Iowa; 1979.
3. Brennen CE. Cavitation and bubble dynamics. New York: Oxford University Press; 1995.
4. Klepetko W, Moritz A, Mlczoch J, Schurawitzki H, Domanig E, Wolner E. Leaflet fracture in Edward–Duromedics bileaflet valves. J Thorac Cardiovasc Surg. 1989;97:90–4.
5. Ericsson A, Lindblom D, Semb G, Huysmans HA, Thulin LI, Scully HE, et al. Strut fracture with Björk–Shily 70° convexo-concave valve: an international multi-institutional follow-up study. Eur J Cardiothorac Surg. 1992;6:339–46.
6. Bottio T, Casarotto D, Thiene G, Caprili L, Angelini A, Gerosa G. Leaflet escape in a new bileaflet mechanical valve: TRI technologies. Circulation. 2003;107:2303–6.
7. Dexter EU, Aluri S, Radcliffe RR, Zhn H, Carlson DD, Heilman TE, et al. In vivo demonstration of cavitation potential of a mechanical heart valve. ASAIO J. 1999;45:436–41.
8. Nakata M, Masuzawa T, Tatsumi E, Taenaka Y, Nishimura T, Tsukiya T, et al. Characterization and optimization of the flow pattern inside a diaphragm blood pump based on flow visualization techniques. ASAIO J. 1998;44:M714–8.
9. Lee HS, Homma A, Tatsumi E, Taenaka Y. Observation of cavitation pits on a mechanical heart valve surface in an artificial heart: in vivo testing. J Artif Organs. 2009;12:105–10.
10. Potthast K, Erdönmen G, Schnelke C, Sellin L, Sliwka U, Schöndube F, et al. Origin and appearance of HITS induced by prosthetic heart valves: an in vitro study. Int J Artif Organs. 2000;23:441–5.
11. Biancucci BA, Deutsch S, Geselowitz DB, Tarbell JM. In vitro studies of gas bubble formation by mechanical heart valves. J Heart Valve Dis. 1999;8:186–96.
12. Zapanta CM, Stinebring DR, Sneckenberger DS, Deutsch S, Geselowitz DB, Tarbell JM, et al. In vivo observation of cavitation on prosthetic heart valves. ASAIO J. 1996;42:M550–5.
13. Sneckenberger DS, Stinebring DR, Deutsch S, Geselowitz DB, Tarbell JM. Mitral heart valve cavitation in an artificial heart environment. J Heart Valve Dis. 1996;5:216–27.
14. Makhijani VB, Yang HQ, Singhal AK, Hwang NHC. An experimental-computational analysis of MHV cavitation:

effect of leaflet squeezing and rebound. J Heart Valve Dis. 1994;3(Suppl I):S35–48.
15. Lee HS, Tatsumi E, Taenaka Y. Effects of the driving condition of a pneumatic ventricular assist device on the cavitation intensity of the inlet and outlet mechanical heart valves. ASAIO J. 2009;55:328–34.
16. Graf T, Reul H, Dietz W, Wilmes R, Rau G. Cavitation of mechanical heart valve under physiologic conditions. J Heart Valve Dis. 1992;1:131–41.
17. Lin HY, Bianccucci BA, Deutsch S, Fontaine AA, Tarbell JM. Observation and quantification of gas bubble formation on a mechanical heart valve. Trans ASME. 2000;122:304–9.
18. Lee HS, Taenaka y. Observation and quantification of cavitation on a mechanical heart valve with an electro-hydraulic total artificial heart. Int J Artif Organs. 2006;29:303–7.

Flow Visualization of A Monoleaflet and Bileaflet Mechanical Heart Valve in A Pneumatic Ventricular Assist Device Using A PIV System

Hwansung Lee, Eisuke Tatsumi, and Yoshiyuki Taenaka

Our group is developing a new type of pulsatile pneumatic ventricular assist device (PVAD) that uses the Medtronic Hall tilting disc valve (M-H valve). Although tilting disc valves have good washout effect inside the blood pump, they are no longer in common clinical use and may be difficult to obtain in the future. To investigate the stability of the Sorin Bicarbon valve (S-B valve) in our PVAD, we constructed a model pump made of an acrylic resin with the same configuration as our PVAD and attempted to compare the flow visualization upstream and downstream of the outlet position valve between the M-H valve and the S-B valve using a particle image velocimetry (PIV) method. The outlet S-B valve had faster closure than the M-H valve. The maximum flow velocity was greater than with the M-H valve. The maximum Reynolds shear stress (RSS) of the M-H valve reached 150 N/m^2 and that of the S-B valve reached 300 N/m^2 upstream during the end-systolic and early-diastolic phases. In both valves, the maximum RSS upstream of the valve was higher than downstream of the valve because of the regurgitation flow during valve closure. In addition, the maximum viscous shear stress reached above 2 N/m^2, which occupied only about 1%–1.5% of the maximum RSS. *ASAIO Journal* 2010; 56:186–193.

The use of a mechanical circulatory support device containing an artificial heart and a ventricular assist device (VAD) has become a standard therapy for bridge to transplantation. In recent years, the most frequently used devices are pulsatile VADs, which use a tilting disc and a tissue valve.[1–3] The flow through the major orifice of the tilting disc valve acts on the blood pump in the diaphragm-housing junction,[4,5] which is good for the washout effect inside the blood pump and helps to prevent thrombosis. However, bileaflet valves have low pressure gradients, central flow, and large effective orifice areas, which have proven superior to the hydrodynamic characteristics of tilting disc valves. Thus, the majority of the mechanical heart valves (MHVs), currently, used clinically have bileaflet valves. Because a bileaflet valve has central flow, it does not allow a good washout flow when installed in a VAD. Moreover, blood cell trauma is caused by shear stress, and the bileaflet valve causes greater shear stress than the tilting disc valve.[6]

Our group is currently developing a new type of pulsatile pneumatic ventricular assist device (PVAD) using the Medtronic Hall valve (M-H valve), a tilting disc valve.[7] However, the M-H valve is no longer commonly used in clinical settings, and it is possible that it will become unavailable in the near future. In a previous study, to select the optimal bileaflet valve for our PVAD, three different valves such as the Advancing The Standard (ATS) valve, St. Jude valve, and Sorin Bicarbon valve (S-B valve) were installed, and we visualized the flow downstream of the outlet valve using a particle image velocimetry (PIV) method.[8] The S-B valve has curved leaflets that cause a reduction of shear stress. Therefore, we used the S-B valve in our PVAD. When using a bileaflet valve in pulsatile VAD, it is important to estimate the thrombus formation within the blood pump and the hemolysis (red cell damage and platelet damage). High shear stress at the valve downstream and leaflet jet leakage and cavitation generated by valve closure are known to be major causes of hemolysis in MHVs.[3–5,9] In previous study, we compared the cavitation intensity between the M-H valve and the S-B valve. Cavitation cycle duration of the M-H valve was 2.54 times than that of the S-B valve.[10] In general, hemolysis due to high shear stresses during valve closing and regurgitation can be higher than that generated during forward flow. However, in previous study, neither shear stress caused by backflow nor shear stress between the M-H valve and the S-B valve was investigated. In this study, we performed flow visualization downstream and upstream of the valves using a PIV method.

In the future, we will use the S-B valve in our PVAD. The purpose of this study was to investigate the stability of the S-B valve in our PVAD. We attempted to compare the shear stress between the M-H valve and the S-B valve to see whether hemolysis occurred using the PIV method.

Materials and Methods

Model Pump

To investigate flow visualization downstream and upstream of the MHV, a model pump unit was constructed of acrylic resin to allow optical access to the internal flow field of the blood pump. It has the same configuration as the PVAD.[7] The model pump was connected to a Donovan mock circulatory loop tester.[11] The mean aortic and left atrial pressures were measured by using a pressure transducer (MP5100, Baxter, Deerfield, IL) with a sampling frequency of 1 kHz, and these pressures were maintained at 100 mm Hg and 7 mm Hg, respectively.

From the Department of Artificial Organs, Research Institute, National Cardiovascular Center, Osaka, Japan.

Submitted for consideration August 2009; accepted for publication in revised form December 2009.

Reprint Requests: Hwansung Lee, Department of Artificial Organs, Research Institute, National Cardiovascular Center, 5-7-1 Fujishirodai, Suita, Osaka 565-8565, Japan. Email: hslee@ri.ncvc.go.jp.

DOI: 10.1097/MAT.0b013e3181d68f83

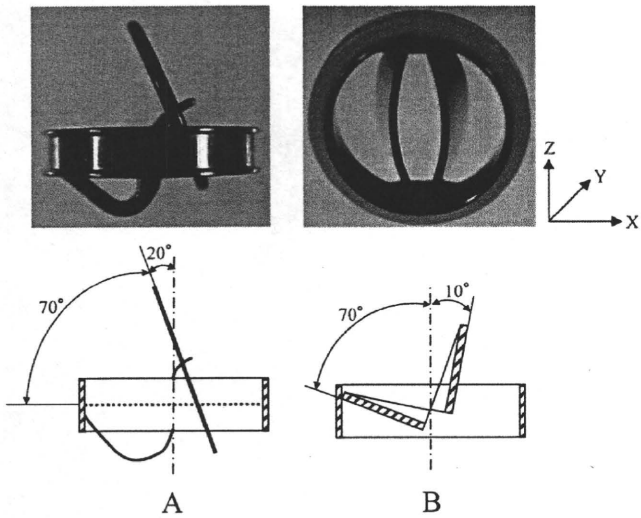

Figure 1. Photograph of the mechanical heart valve. **A:** 23-mm M-H valve; It has an orifice diameter of 18 mm, an internal orifice area of 2.54 cm^2 and an opening angle of 70°; **B:** 23-mm S-B valve; it has an orifice diameter of 18.7 mm, an internal orifice area of 2.8 cm^2 and an opening angle of 60°.

Testing Valve

A 23-mm Medtronic Hall valve (M-H valve, Medtronic, Inc., Minneapolis, MN) and a 23-mm Sorin Bicarbon valve [S-B valve, Sorin Biomedica Cardio S.p.A., Saluggia (VC), Italy] were each mounted on the model pump (**Figure 1**). The major orifice direction of the M-H valve and S-B valve were set at a 180° clockwise orientation in the inlet port. In addition, the major orifice direction of the M-H valve and S-B valve were set at a 180° and 0° clockwise orientation in the outlet port.

The model pump was operated at a positive pressure of 230 mm Hg and a negative pressure of −50 mm Hg using a control-drive console for circulatory support (VCT-30; Toyobo, Osaka, Japan). The model pump ran at a heart rate of 70 beats/min and systolic duration of 35%, with a bypass flow of 4.5 L/min. The blood analog fluid was a mixture of 50% water and 50% glycerol by volume and had a viscosity coefficient of 3.4 cP and a density of 1.12 g/cm^3 at 37°C. Bypass flow was measured with an ultrasound flow meter (T106; Transonic Systems, Ithaca, NY) at the outflow side.[8] A charge-coupled device laser displacement sensor (LK-080, Keyence, Osaka, Japan) with a sampling frequency of 1 kHz was used to measure the opening and closing behavior of the leaflet.[8]

PIV Method[8]

A polystyrene tracer with a diameter of 50 μm and a density of 1.06 g/cm^2 (Vestosint; Degussa AG, Düsseldorf, Germany) was added to the fluid. In a previous study, we could not observe the optical distortion caused by the different densities of the working fluid and polystyrene tracer. A dual Nd: YAG laser system (Solo II-15, New Wave Research Inc, Fremont, CA) with a 30 mJ/pulse at a 532-nm wavelength and a pulse width of 3–5 ns was used as the flow visualization. The PIV images were taken by using a high-speed camera with 1,008×1,024 pixels and a 9 μm/pixel square spacing (PIVCAM 10–30, TSI, Inc., Shoreview, MN). It was operated at a frame rate of 30 Hz, with a shutter open time of 200 μs.

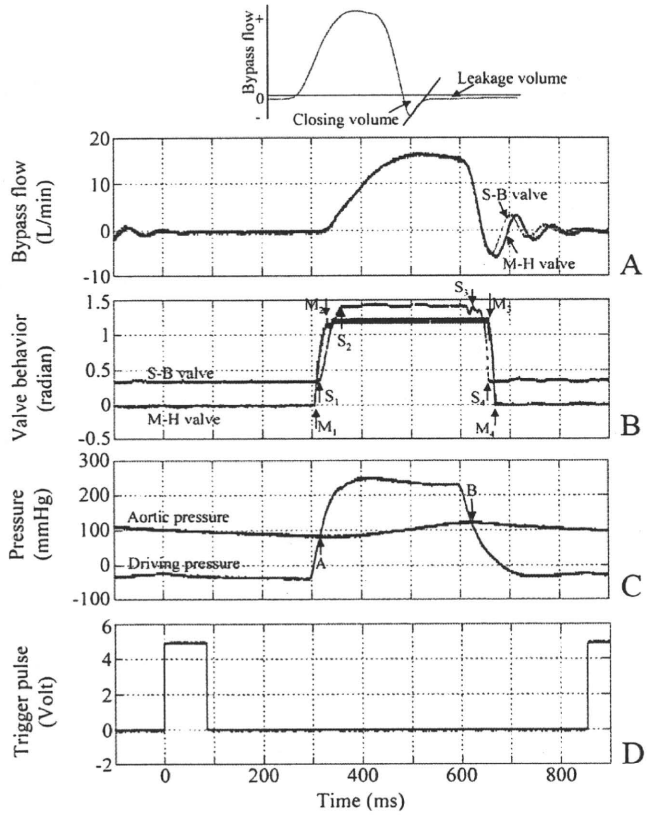

Figure 2. Bypass flow, aortic and driving pressure, outlet valve behavior and trigger pulse waves. **A:** Bypass flow; **B:** Outlet valve behavior; **C:** Driving and aortic pressures; **D:** Trigger pulse. The time domain of 0 ms of the horizontal axis is the trigger point of the synchronizer and the ECG-R mode of the control-drive console for circulatory support. The time domain of 0 ms was the trigger point of the synchronizer and the ECG-R mode of the control-drive console for circulatory support.[10] The time domain between 300 ms and 375 ms is the early-systolic phase, between 375 ms and 525 ms the mid-systole phase, between 525 ms and 600 ms the end-systolic phase, and between 600 ms and 700 ms the early-diastolic phase.

The laser sheet illuminated two different planes, the X-Y plane and the X-Z one. The flow velocity vector was measured using PIV software (Insight 3G; version 9.0, TSI, Inc., Shoreview, MN), and its vector files were loaded into the Tecplot Focus 2008 (Tecplot, Inc., Bellevue, WA). We used a recursive Nyquist grid with a starting spot dimension of 64×64 pixels and a final spot dimension of 32×32 pixels. In addition, we used the Fast Fourier Transform correlate as the correlation engine and the Gaussian peak as the peak engine. A function generator to provide a square pulse was used as the trigger signal of the synchronizer (Model 610034, TSI, Inc., Shoreview, MN), and the ECG-R (electrocardiogram-R wave) mode of the control-drive console was used for circulatory support. The PIV images of 100 cycles were averaged for each of the experiment points.

Results

The peak bypass flow was reached at ~17 L/min in both valves, and the closing volume of the M-H valve was greater than that of the S-B valve (**Figure 2A**). In the case of the M-H valve, 0 radian of the valve behavior indicated the valve had

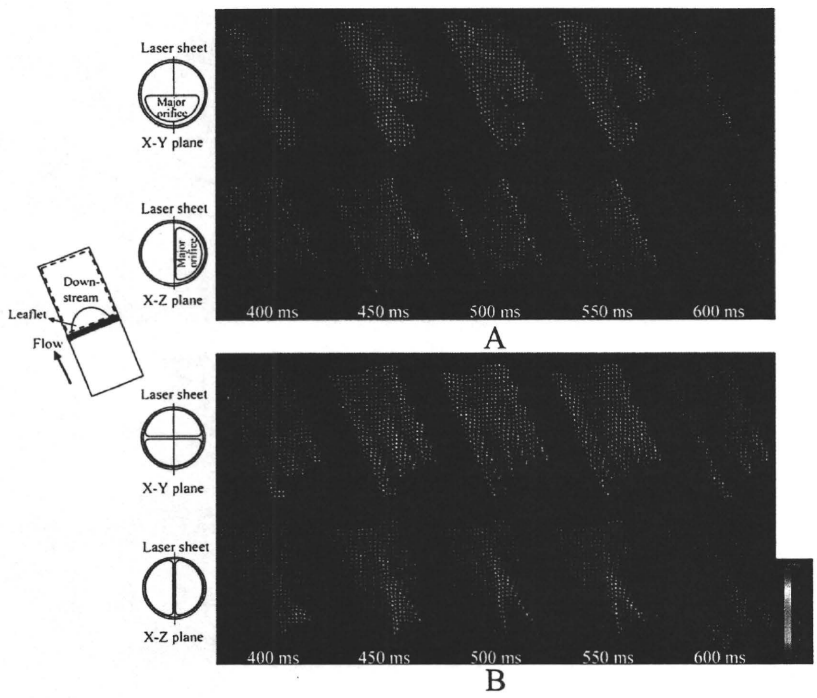

Figure 3. Vector field of the flow-velocity of the valve downstream. **A:** M-H valve; **B:** S-B valve. A large flow was observed from the major orifice at the M-H valve in the X-Y plane, whereas a smaller flow was observed from the minor orifice in the X-Y plane during the mid-systolic phase (between 450 ms and 550 ms). At the S-B valve in the X-Y plane, there are three regions of high flow velocity: two lateral orifices and a central orifice during the mid-systolic phase (between 450 ms and 550 ms). At the S-B valve in the X-Z plane, a high flow velocity was observed at the central orifice.

closed, and 1.2 radians of the valve behavior indicated the valve had opened completely (**Figure 2B**). Because the S-B valve has a 20° angle when it is completely closed, 0.35 radian of the vertical axis of **Figure 2B** indicated the valve was completely closed and 1.4 radians indicated the valve was completely opened. The outlet M-H valve opened ("M_1" of **Figure 2B**) before the driving pressure exceeded the aortic pressure ("A" of **Figure 2C**). When the driving pressure exceeded the aortic pressure ("A" of **Figure 2C**), the outlet S-B valve opened ("S_1" of **Figure 2B**). In addition, the outlet M-H valve started closing ("M_3" of **Figure 2B**) after the driving pressure fell under the aortic pressure ("B" of **Figure 2C**). The outlet S-B valve started closing ("S_3" of **Figure 2B**), when the driving pressure fell under the aortic pressure ("B" of **Figure 2B**). The outlet of the S-B valve closed faster than the outlet of the M-H valve (**Figure 2B**).

Downstream of the M-H valve in the X-Y plane, a large flow was observed from the major orifice, whereas a smaller flow was observed from the minor orifice in the X-Y plane during the mid-systolic phase (between 450 ms and 550 ms in **Figure 3A**). These two different flow velocities induced a recirculation flow in the wake of the leaflet during the end-systolic phase (600 ms in **Figure 3A**). However, a high-speed flow was not observed at the M-H valve in the X-Z plane. At the downstream of the S-B valve in the X-Y plane, there are three regions of high flow velocity: two lateral orifices and a central orifice during the mid-systolic phase (between 450 ms and 550 ms in **Figure 3B**). The different flow velocity between the lateral orifice and central orifice induced a recirculation flow during the end-systolic phase (600 ms in **Figure 3B**). Moreover, at the S-B valve in the X-Z plane, a high-flow velocity was observed at the central orifice, but a recirculation flow was observed between the wall and central orifice during the end-systolic phase (600 ms in **Figure 3B**). Upstream of both valves, a recirculation flow was observed in both planes during the end-systolic phase (**Figure 4**).

The maximum flow velocity downstream is shown in **Figure 5**. The maximum flow velocity in both valves reached about 2 m/s at the X-Y plane (**Figure 5A**). At the X-Z plane, the maximum flow velocity of the S-B valve reached 2.1 m/s, but the M-H valve reached only 1.6 m/s (**Figure 5B**). In both the X-Y and X-Z planes, the maximum flow velocity of the S-B valve was higher than that of the M-H valve (**Figure 5**).

Downstream of the M-H valve, high Reynolds shear stress (RSS) was not observed at either the X-Z or X-Y plane. However, high RSS was observed near the leaflet of the S-B valve at the X-Y plane and central line at the X-Z plane during the mid-systolic phase (**Figure 6**). Upstream in both valves, high RSS was observed near the leaflet and the wall during the end-systolic and early-diastolic phases (between 550 ms and 625 ms in **Figure 7**). Along the X-Y plane in both valves, the maximum RSS reached 120 N/m^2 downstream during the mid-systolic phase (450 ms in **Figure 8A**). Conversely, the maximum RSS reached above 150 N/m^2 upstream during the end-systolic and early-diastolic phases (between 600 ms and 630 ms in **Figure 8B**). In particular, the peak maximum RSS of the S-B valve was higher than that of the M-H valve (**Figure 8A**). Along the X-Z plane in both valves, the maximum RSS reached 150 N/m^2 downstream during the mid-systolic phase (450 ms in **Figure 8B**). However, the maximum RSS reached above 200 N/m^2 upstream during the early-diastolic phase (between 625 ms and 630 ms in **Figure 8B**). The peak maximum RSS of the S-B valve was greater than that of the M-H valve, which reached 300 N/m^2 (**Figure 8B**).

Downstream of the M-H valve, high viscous shear stress (VSS) was observed near the wall in both planes during the mid-systolic phase (between 450 ms and 550 ms in **Figure 9A**). Downstream of the S-B valve, high RSS was observed near the leaflet at the X-Y plane and central line at the X-Z plane during the mid-systolic phase (between 450 ms and 550 ms in **Figure 9B**).

Upstream of the S-B valve, high VSS was observed near the wall during the end-systolic phase (between 550 ms and 575 ms in **Figure 10**). Upstream in both valves, high VSS was

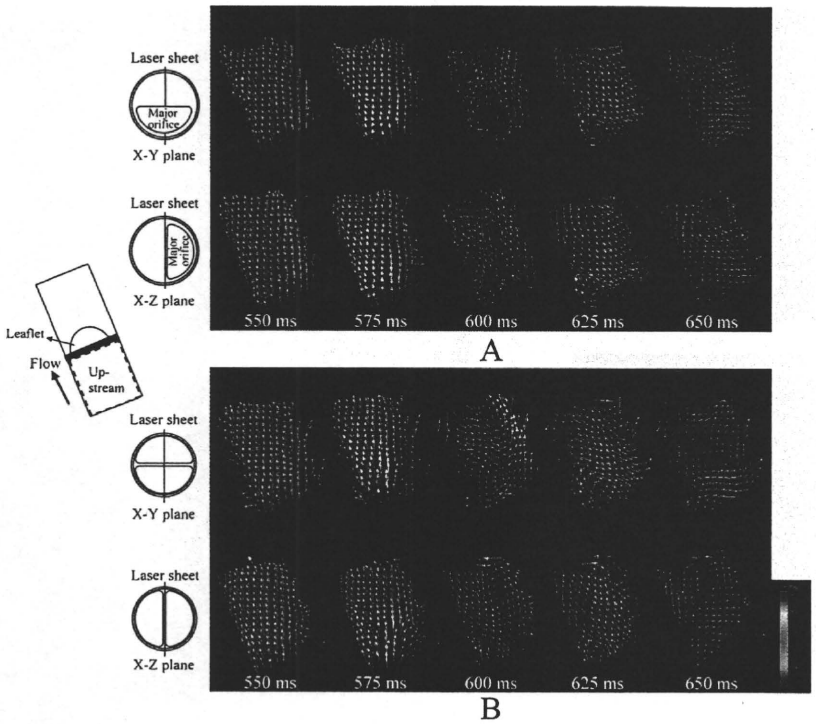

Figure 4. Vector field of the flow-velocity of the valve upstream. **A:** M-H valve; **B:** S-B valve. In both valves, a recirculation flow was observed in both planes during the end-systolic phase.

observed near the leaflet (600 ms in **Figure 10**), which might have occurred because of the regurgitation flow during the end-systolic phase. Along the X-Y plane in both valves, the maximum VSS reached 1.3–1.5 N/m^2 downstream and was greater at the S-B valve than at the M-H valve (**Figure 11A**). The maximum VSS of the S-B valve upstream reached about 2 N/m^2 (**Figure 11A**). Along the X-Z plane of the M-H valve, the maximum VSS reached only 1 N/m^2 downstream (**Figure 11B**). The maximum VSS of the S-B valve downstream and the M-H valve upstream reached about 2.5 N/m^2. In both valves, the maximum VSS occupied only 1%–1.5% of the maximum RSS of **Figure 8**.

Discussion

The PIV method enables adequate temporal and spatial resolution to estimate flow velocity fields and is thus a powerful tool for studying and estimating thrombus formation inside the blood pump and the hemolysis that occurs in medical devices. Kaminsky *et al.*[9,12] investigated the flow visualization through a bileaflet and monoleaflet valve using the stereoscopic high-speed PIV method. They reported that in the case of a bileaflet valve, the maximum velocity is ~1.3 m/s. However, in a monoleaflet valve, the highest velocity of 0.7 m/s was observed near the tip of the leaflet. Kaminsky *et al.* investigated the flow visualization effect on the sinus cavity and considered the implantable MHV condition in a natural heart. In this study, the valves were installed on the VAD, and there was, thus, no compliance to the natural heart required, and the maximum flow velocity of the valves was, therefore, greater than that found in the Kaminsky group's study. However, the maximum flow velocity of the monoleaflet valve was less than that of the bileaflet valve, the same result as obtained by Kaminsky.

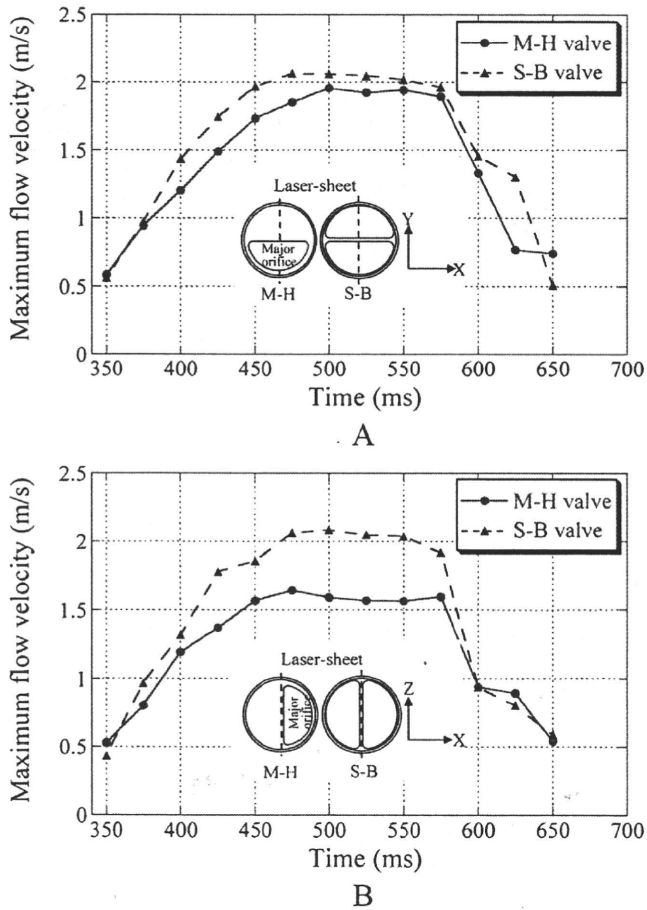

Figure 5. Maximum flow velocity at the valve downstream. **A:** X-Y plane; **B:** X-Z plane. In both the X-Y and X-Z planes, the maximum flow velocity of the S-B valve was higher than that of the M-H valve.

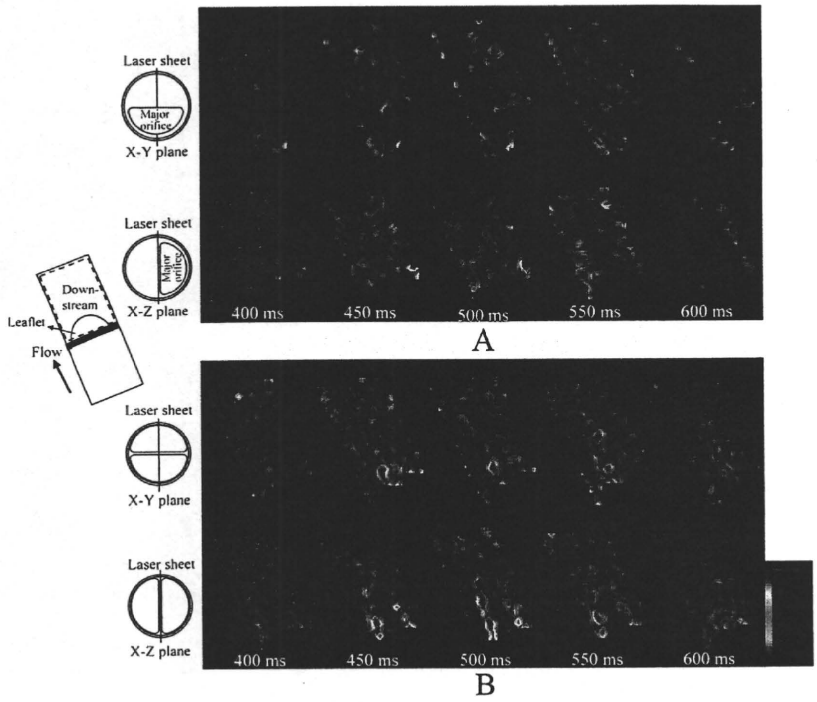

Figure 6. Reynolds shear stress field of the valve downstream. **A:** M-H valve; **B:** S-B valve. High Reynolds shear stress was not observed at the M-H valve, however was observed near the leaflet of the S-B valve.

In previous study, we investigated the shear stress downstream of three types of commercially available bileaflet valves. However, hemolysis due to high shear stresses during valve closing and regurgitation can be higher than that generated during forward flow. In this study, we performed flow visualization downstream and upstream of the valves using a PIV method. There is a different flow pattern at the valve open phase between the monoleaflet valve (M-H valve) and the bileaflet valve (S-B valve). Because of the geometry of the valve, the S-B valve has a larger field of high flow velocities than the M-H valve (**Figure 5**). This is a major cause of the occurrence of the large recirculation flow and high shear stress in the S-B valve. Moreover, as shown in **Figure 2B**, the S-B valve has two leaflets, and their closure was faster than the monoleaflet closure of the M-H valve. This faster closure motion might be caused by high shear stress. We confirmed that high shear stress was generated upstream in both valves.

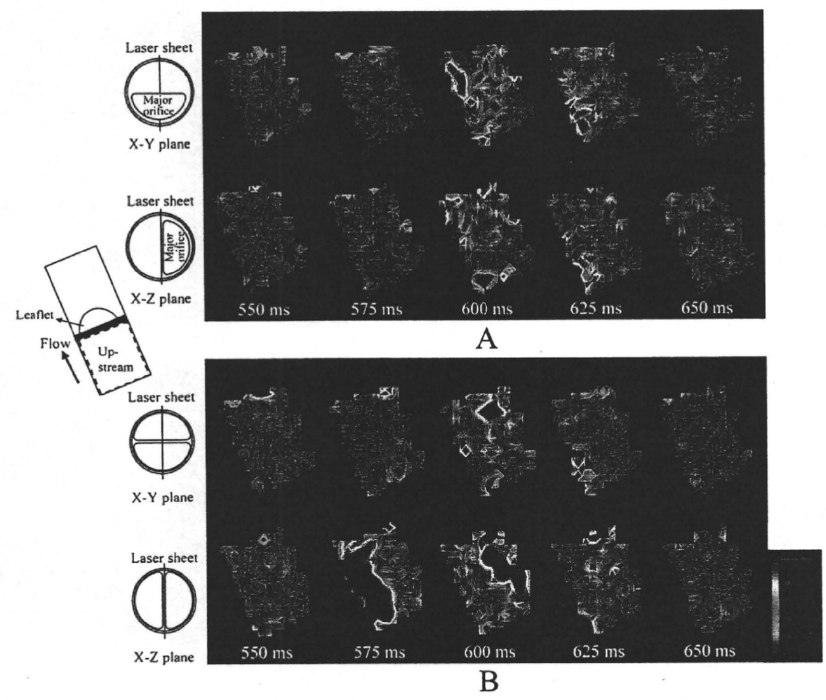

Figure 7. Reynolds shear stress field of the valve upstream. **A:** M-H valve; **B:** S-B valve. High Reynolds shear stress (RSS) was observed near the leaflet and the wall in both valves.

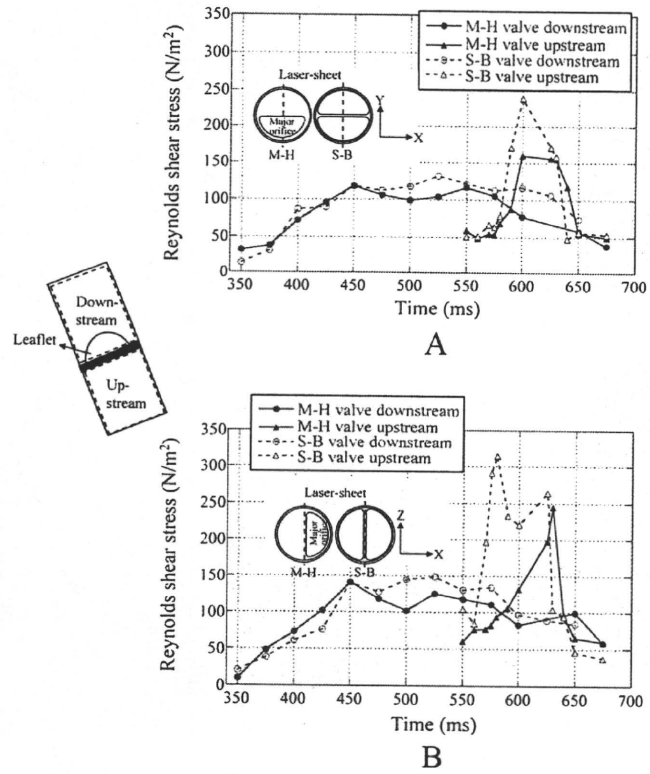

Figure 8. Maximum Reynolds shear stress in both valves. **A:** X-Y plane; **B:** X-Z plane. Along the X-Y plane, the peak maximum Reynolds shear stress (RSS) of the S-B valve was higher than that of the M-H valve. Along the X-Z plane, the peak maximum RSS of the S-B valve was greater than that of the M-H valve.

Hemolysis (red cell damage and platelet damage) is a function of exposure time and shear stress.[13] Leverett *et al.*[13] reported that the threshold level for red blood cell damage because of shear stress is ~150 N/m^2 and an exposure time of 102 s. Sallam *et al.*[14] reported that hemolysis requires shear stress of 400 N/m^2 during exposure time through a heart valve of 1 ms. The platelets are much more sensitive to shear stress than red blood cells, and the shear stress threshold for platelet damage is ~10 N/m^2.[15] In this study, we found that the maximum RSS of the S-B valve was higher than that of the M-H valve. Moreover, in both valves, the maximum RSS upstream of the valve was higher than downstream of the valve and was caused by the regurgitation flow during the valve closure. This means that the shear stress upstream of the valve can cause hemolysis. However, the maximum RSS of the S-B valve ranged from 150 to 250 N/m^2, which was found to be well below the range required to inflict damage to red blood cells, but exceeded the threshold for platelet damage of 10 N/m^2. Upstream in both valves, high VSS was observed near the leaflet during the end-systolic phase (**Figure 10**), which was caused by the leakage jet. However, the maximum VSS reached 2.5 N/m^2, which occupied only 1%–1.5% of the maximum RSS and was below the threshold for platelet damage. The RSS was used to determine whether hemolysis was caused by the valve-induced flow turbulence.

High shear stress is caused by activated platelets, which then get trapped in the recirculation regions, where platelet-to-platelet contact is enhanced and where thrombus formation may occur.[16] In monoleaflet and bileaflet valves, a recirculation flow pattern forms in the sinus region.[16] In this study, high shear stress was observed near the leaflets. Our PVAD has no sinus, and there is, therefore, no possibility of thrombus formation occurring. However, the bileaflet valve has a hinge where stagnant flow regions occur during the leakage flow phase, and thus where thrombus formation might occur. Bluestein reported that the bileaflet valve in a VAD promoted the platelet activation state, which is a major cause of thromboembolism inside a VAD.[17] In the future, we will be investi-

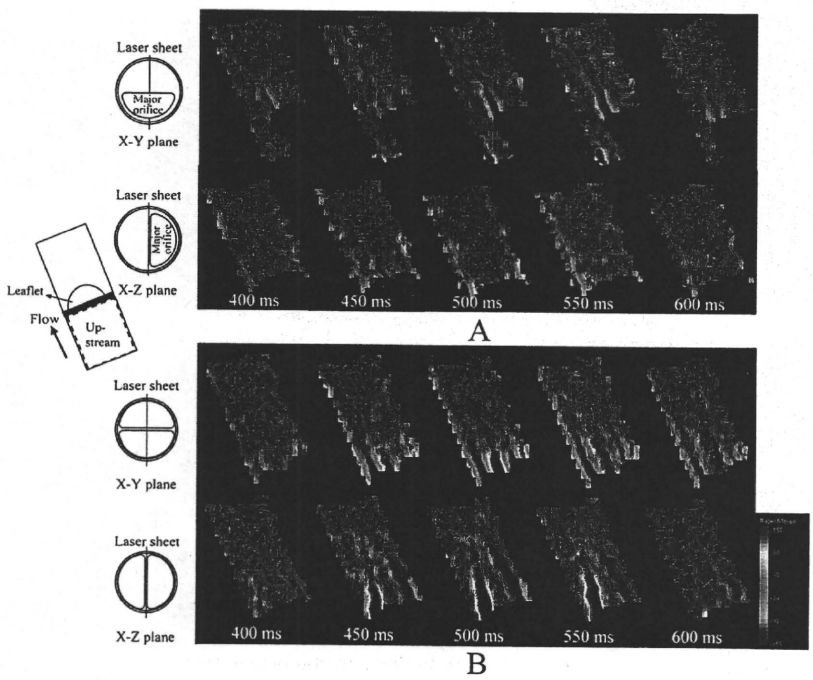

Figure 9. Viscous shear stress (VSS) field of the valve downstream. **A:** M-H valve; **B:** S-B valve. At the M-H valve, high VSS was observed near the wall in both planes. At the S-B valve, high Reynolds shear stress (RSS) was observed near the leaflet at the X-Y plane and central line at the X-Z plane.

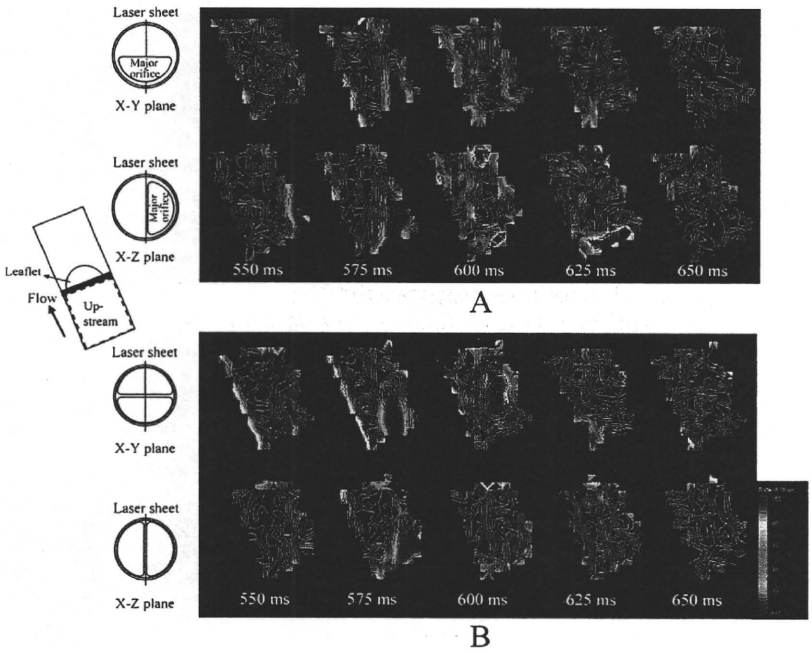

Figure 10. Viscous shear stress (VSS) field of the valve upstream. **A:** M-H valve; **B:** S-B valve. High VSS was observed near the wall during the end-systolic phase at the S-B valve and was observed near the leaflet in both valves.

gating the possibility of thrombus formation in our PVAD using *in vivo* testing.

As a next step, we will conduct blood bag tests to quantify hemolysis in the different MHVs. Finally, to estimate hemolysis of S-B valve and thrombosis within the pump, we will investigate free plasma hemoglobin as index of hemolysis in MHVs and thrombus formation within the pump using long-term animal experiment.

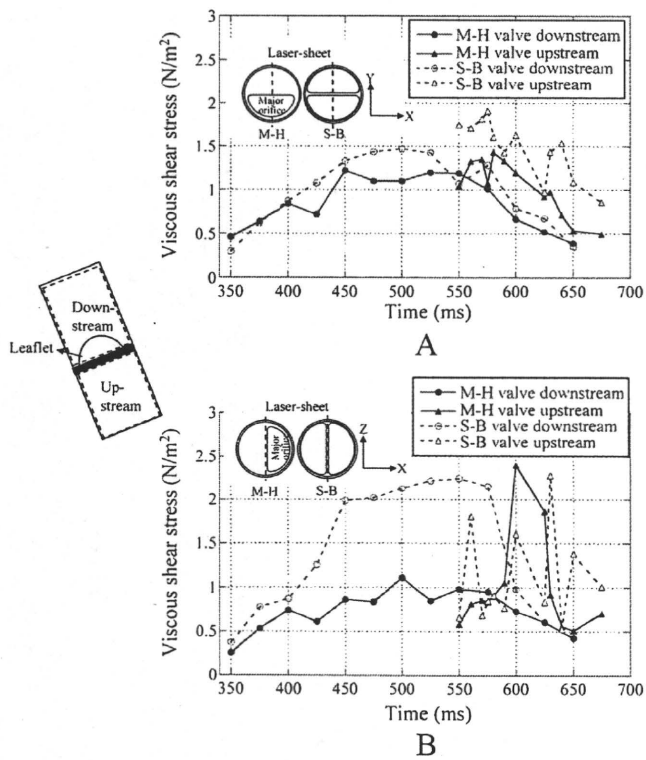

Figure 11. Maximum viscous shear stress (VSS) in both valves. **A:** X-Y plane; **B:** X-Z plane. In both valves, the maximum VSS occupied only 1%–1.5% of the maximum Reynolds shear stress.

Conclusion

In this study, we attempted to compare flow visualization upstream and downstream of the outlet position valve between the M-H valve and the S-B valve using a PIV method. The maximum RSS of the S-B valve was greater than that of the M-H valve. In both valves, the maximum RSS upstream of the valve was higher than downstream of the valve because of the regurgitation flow during the valve closure. In addition, the maximum VSS reached above 2 N/m^2, which occupied only about 1%–1.5% of the maximum RSS. The RSS upstream of the valve might be a very important factor when estimating MHV hemolysis in an artificial heart.

Acknowledgment

This work was supported by the Program for the Promotion of Fundamental Studies in Health Science of the National Institute of Biomedical Innovation (NIBIO).

References

1. Stevenson LW, Kormos RL: Mechanical cardiac support 2000: Current applications and future trial design. *J Am Coll Cardiol* 37: 340–370, 2001.
2. Bachmann C, Hugo G, Rosenberg G, *et al*: Fluid dynamic of a pediatric ventricular assist device. *Artif Organs* 24: 362–372, 2000.
3. Manning KB, Wivholm BD, Yang N, *et al*: Flow behavior within the 12-cc Penn State pulsatile pediatric ventricular assist device: An experimental study of the initial design. *Artif Organs* 32: 442–452, 2008.
4. Nakata M, Masuzawa T, Tatsumi E, *et al*: Characterization and optimization of the flow pattern inside a diaphragm blood pump based on flow visualization techniques. *ASAIO J* 44: M714–M718, 1998.

5. Akagawa E, Lee HS, Tatsumi E, *et al*: Effects of mechanical valve orifice direction on flow pattern in a ventricular assist device. *J Artif Organs* 10: 85–91, 2007.
6. Yoganathan AP, Woo YR, Sung HW: Turbulent shear stress measurements in the vicinity of aortic heart valve prostheses. *J Biomech* 19: 433–442, 1986.
7. Lee HS, Tatsumi E, Taenaka Y: Effects of the driving condition of a pneumatic ventricular assist device on the cavitation intensity of the inlet and outlet mechanical heart valves. *ASAIO J* 55: 328–334, 2009.
8. Lee HS, Tatsumi E, Taenaka Y: Experimental study on the Reynolds and viscous shear stress of bileaflet mechanical heart valves in a pneumatic ventricular assist device. *ASAIO J* 55: 348–354, 2009.
9. Kaminsky R, Kallweit S, Weber HJ, *et al:* Flow visualization through two types of aortic prosthetic heart valves using stereoscopic high-speed particle image velocimetry. *Artif Organs* 31: 869–879, 2007.
10. Lee HS, Akagawa E, Tatsumi E, et al: Characteristics of cavitation intensity in a mechanical heart valve using a pulsatile device: Synchronized analysis between visual images and pressure signals. *J Artif Organs* 11: 60–66, 2008.
11. Donovan FM: Design of a hydraulic analog of the circulatory system for evaluating artificial hearts. *Biomater Med Devices Artif Organs* 3: 439–449, 1975.
12. Kaminsky R, Morbiducci U, Rossi M, *et al*: Time-resolved PIV technique for high temporal resolution measurement of mechanical prosthetic aortic valve fluid dynamics. *Int J Artif Organs* 30: 153–162, 2007.
13. Leverett LB, Hellums JD, Alfrey CP, *et al:* Red blood cell damage by shear stress. *Biophysical J* 12: 257–273, 1972.
14. Sallam AM, Hwang NHC: Human red blood cell hemolysis in a turbulence shear flow: contribution of Reynolds shear stresses. *Biorheology* 21: 783–797, 1984.
15. Ge L, Dasi LP, Sotiropoulos F, *et al*: Characterization of hemodynamic forces induced by mechanical heart valve: Reynolds vs. viscous stresses. *Ann Biomed Eng* 36: 276–297, 2008.
16. Dasi LP, Simon HA, Sucosky P, *et al*: Fluid mechanics of artificial heart valve. *Clin Exp Pharmacol Physiol* 36: 225–237, 2009.
17. Bluestein D: Research approaches for studying flow-induced thromboembolic complications in blood recirculating devices. *Expert Rev Med Devices* 1: 65–80, 2004.

医療機器の研究開発の促進への取り組み
—先端医療開発特区（スーパー特区）の構築—

妙中　義之*

医薬品医療機器レギュラトリーサイエンス
Vol. 41, No. 8　別刷（2010年）
財団法人　日 本 公 定 書 協 会